PAPER • OPEN ACCESS

Technology for detecting spectral radiance by a snapshot multi-imaging spectroradiometer

To cite this article: Ralf Zuber *et al* 2017 *Meas. Sci. Technol.* **28** 125903

View the article online for updates and enhancements.

Technology for detecting spectral radiance by a snapshot multi-imaging spectroradiometer

Ralf Zuber[1,3] , **Ansgar Stührmann**[2]**, Anton Gugg-Helminger**[1] **and Gunther Seckmeyer**[2]

[1] Gigahertz-Optik GmbH, An der Kälberweide 12, 82299 Türkenfeld/Munich, Germany
[2] Institut für Meteorologie und Klimatologie, Leibniz Universität Hannover, Herrenhäuser Str. 2, 30419 Hannover, Germany

E-mail: r.zuber@gigahertz-optik.de

CrossMark

Abstract

Technologies to determine spectral sky radiance distributions have evolved in recent years and have enabled new applications in remote sensing, for sky radiance measurements, in biological/diagnostic applications and luminance measurements. Most classical spectral imaging radiance technologies are based on mechanical and/or spectral scans. However, these methods require scanning time in which the spectral radiance distribution might change. To overcome this limitation, different so-called snapshot spectral imaging technologies have been developed that enable spectral and spatial non-scanning measurements. We present a new setup based on a facet mirror that is already used in imaging slicing spectrometers. By duplicating the input image instead of slicing it and using a specially designed entrance slit, we are able to select nearly 200 (14×14) channels within the field of view (FOV) for detecting spectral radiance in different directions. In addition, a megapixel image of the FOV is captured by an additional RGB camera. This image can be mapped onto the snapshot spectral image. In this paper, the mechanical setup, technical design considerations and first measurement results of a prototype are presented. For a proof of concept, the device is radiometrically calibrated and a $10\,mm \times 10\,mm$ test pattern measured within a spectral range of 380 nm–800 nm with an optical bandwidth of 10 nm (full width at half maximum or FWHM). To show its potential in the UV spectral region, zenith sky radiance measurements in the UV of a clear sky were performed. Hence, the prototype was equipped with an entrance optic with a FOV of 0.5° and modified to obtain a radiometrically calibrated spectral range of 280 nm–470 nm with a FWHM of 3 nm. The measurement results have been compared to modeled data processed by UVSPEC, which showed deviations of less than 30%. This is far from being ideal, but an acceptable result with respect to available state-of-the-art intercomparisons.

Keywords: spectral snapshot imaging, sky radiance, snapshot multi-imaging spectroradiometer, spectroradiometer

(Some figures may appear in colour only in the online journal)

[3] Author to whom any correspondence should be addressed.

1. Introduction

Historically, technologies for assessing spectral imaging radiance data (also called hyperspectral imaging) are based on scanning in either the spectral (Hardeberg *et al* 2002, Gupta and Voloshinov 2004, Mathews 2008, Sigernes *et al* 2012) or spatial domain (Hu *et al* 2005). However, non-scanning, so-called snapshot spectral imaging technologies have become more popular in recent years (Content 1997, Matsuoka *et al* 2002, Henault *et al* 2004, Laurent *et al* 2006, Gehm *et al* 2007, Wagadarikar *et al* 2008, Gao *et al* 2010, Riechelmann *et al* 2013). These technologies allow time-resolved investigations of, e.g. cloud movements in atmospheric science, OLED (organic light emitting diode) panel investigations, chemical process analysis, mineralogy of planet surfaces (Brown *et al* 2010) and many more applications (Brown 2006). A detailed overview of the known spectral snapshot imaging technologies and applications is given in (Hagen and Kudenov 2013). In the following paragraph, a short appraisal is presented to explain the important differences between spectral-scanning, mechanical-scanning and spectral snapshot measurements (figure 1).

Spectral scans (figure 1, second from left) are achieved using, for example optical filter glasses, acousto-optical filters or interferometers. The spectral resolution and spectral domain of this approach is determined by the filtering technology and the measurement time. For higher resolution, a large number of measurements is needed. Furthermore, in some wavelength regions like the UV, only a few types of filters are available whereby the optical performance is limited. However, the advantage of these technologies is a very high spatial resolution since, in principle, high-resolution photographic cameras can be used (Bianco *et al* 2010). Mechanical scans (figure 1, point scanning on the left or line-scanning second from right) vary the field of view (FOV) by either moving the whole spectroradiometer (e.g. remote sensing with the help of satellites or aircraft) or by using mirror-based scanners. As a result, the spatial resolution of point-scanning devices (1D array detector) in both dimensions (x, y) depends on the number of scans. When using line-scanning devices (2D array detector), one spatial dimension (e.g. x) depends on the number of scans, the other (e.g. y) on the number of pixels that can be resolved by the device within the measurement line. This technology is also called push-broom scanning (Davis *et al* 2002, Brown *et al* 2008). Hence, the spatial resolution is limited by the measurement time. The advantage of this technology is based on the freedom in the choice of the spectrometer design and performance.

However, all scanning technologies have the common disadvantage that time-resolved effects can only be analyzed when they are significantly slower than the scanning itself. Spectral and point-scanning measurements take time and thus fast temporal effects like cloud movement cannot be resolved.

To analyze such kind of tasks, snapshot spectral imaging technologies are needed. One of many existent approaches is based on imaging a coded spatial and spectral information mixture on the detector and mathematically reconstructing the spectral snapshot image (Gehm *et al* 2007, Wagadarikar *et al* 2008). Another approach is the so-called integral field spectroscopy (IFS) snapshot technology, such as fiber bundle-based technologies (IFS-F), where single fibers capture the signal of one measurement channel (Hagen and Kudenov 2013). These fibers are lined up on the entrance slit of a line-scanning spectrometer. Subsequently, the maximum spatial resolution is limited by the number of fibers that can be mechanically lined up and optically imaged without channel crosstalk on the detector. A higher resolution system has been achieved by Riechelmann *et al* (2013) with a spatial resolution of 113 channels. Furthermore, a couple of image slicing spectrometer (ISS) technologies (one example being IFS-M) are known for applications in astronomy or for microscopy purposes (Content 1997, Henault *et al* 2004, Laurent *et al* 2006, Gao *et al* 2009). These approaches are based on a facet mirror optical design, which slices the image into single parts that are spectrally resolved.

In this paper, a new type of IFS approach is presented. A facet mirror is used to produce duplicated images instead of slicing the image as with known IFS-M technologies. For the spatial resolution, different parts of each duplicated image are selected by the entrance slit of a line-scanning spectrometer. These parts are spectrally resolved and can be rearranged by software to obtain the spectral snapshot image afterwards. In addition, a RGB camera can take a high resolution image of one duplicated image by the facet mirror. These data can be used as meta information to simplify further data analysis. For example, the image can be mapped to the lower resolution spectral snapshot imaging data.

The new design is based on very few optical parts and a well-known line-scanning spectrometer with freedom in design of spectral range, spectral resolution and optical bandwidth (full width at half maximum or FWHM Seckmeyer *et al* (2001)). The new system is called 4D Imager since measurements of an image (2D), spectral resolution (1D) and snapshot in time (1D) with well-balanced performance in all four dimensions could be achieved.

1.1. Fundamental concept of the 4D Imager

The essential part of the 4D Imager is a facet mirror (figure 2(b)), which is reflecting the incoming image (figure 2(a)) in different directions. The reflection angle α depends on the specific facet angle β:

$$\alpha = 2 \cdot \beta. \tag{1}$$

As shown in figure 2 with one larger mirror (figure 2(c)), these signals can be imaged at the image plane d. Depending on their reflecting angle α, multiple images are generated since they are lined up as duplicated images in the imaging plane (figure 2(d)) in different heights h. The height h depends on the reflection angle α, focal length of the mirror, object and imaging distance. These quantities can be determined by the well-known imaging formulas. For gathering further information about the object, one part of the signal can imaged on an additional camera to obtain a higher spatial resolution image (figure 2(e)).
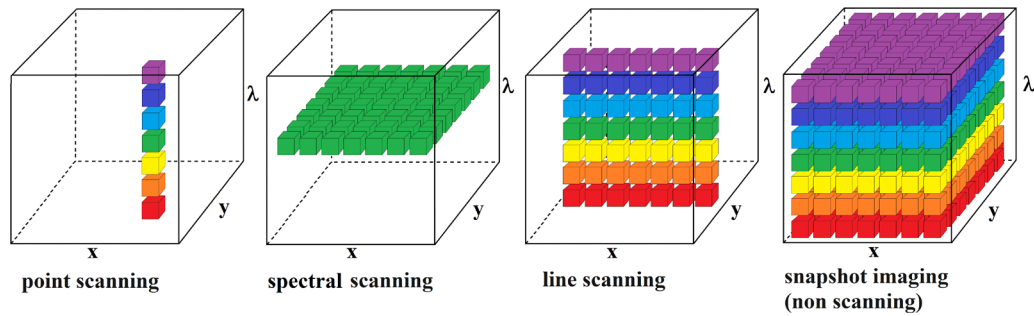
Figure 1. Schematical overview of different type of imaging spectrometer technologies.

The lined up images (figure 2(d)) are physically identical and contain the same information. The number of images is determined by the number of facets. In order to extract different information, or parts, out of each image, a customized aperture is used. After the aperture, the lined up image parts enter a well-known line-scanning spectrometer and can be spectrally resolved. Due to a fixed correlation between the slit position and image pixel, the measured data can be rearranged to get the spectral snapshot image voxels (x, y, λ). This imaging process is schematically shown in figure 3.

This technology has been successfully patented (Zuber 2015).

2. Design considerations

The size and angle of the mirror facets have to be chosen in such a way that they fit to the whole spectrometer design. The number of facets m of the facet mirror defines the spatial nominal resolution in one dimension (e.g. x). The spatial resolution in the other dimension (y) is given by the following formula:

$$y = \frac{n}{m} - u, \tag{2}$$

where n represents the number of pixels, which can be resolved spectrally by the line-scanning spectrometer. u is a parameter depending on the system design and represents the amount of pixels that cannot be used per measurement (see figure 3(e)). The width of the single slits of the customized aperture (figure 3(c)) is not only determining the part of the image that is selected, it directly affects the optical bandwidth (FWHM) since it represents the entrance slit of the spectrometer. The spectral range and resolution of this technology only depends on the design of the line-scanning spectrometer (l/mm of the grating, etc). Due to the image duplication and selection process, the entrance slit of the spectrometer is shaped like a saw tooth (figure 3(c)). This directly affects the spectral range, which is slightly shifted (o_n) at each set of channels (figure 3(e)). In terms of alignment, the key task of this technology is the mapping of the customized aperture (figure 3(c)) to the duplicated images (figure 3(b)). Tilts, rotation, and a shifting of the aperture would directly lead to an incorrect selection of spatial pixels of the duplicated images.
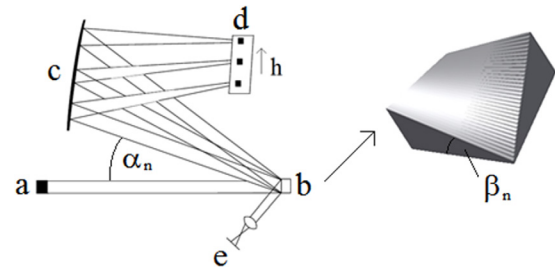
Figure 2. Left side: Principal path of the imaging rays. (a) The FOV, (b) the facet mirror, (c) the imaging mirror, (d) the imaging plane and (e) the additional high resolution camera. Right side: Facet mirror; each facet has a different angle β.

3. Characterization of the 4D Imager prototype

In order to perform proof of concept measurements, a 4D Imager prototype has been developed and configured for the visible spectral region with a spatial resolution of 14×14 channels. The measurement object is a $10\,\text{mm} \times 10\,\text{mm}$ test pattern with a distance of 1 m. An additional facet is used to provide a spatially higher resolution image, captured with an RGB camera.

The prototype is based on UV enhanced mirrors (Edmund Optics) and optical gratings (Newport) from stock. As a detector a Princeton Instruments Pixis 400B has been choosen. As a RGB camera, for the additional image, a AVT MAKO G-125C POE was used. The facet mirror has been produced by Gigahertz-Optik GmbH.

In the following, the calibration steps of this setup and measurement results are presented.

3.1. Channel calibration (object position to detector position)

The incoming signal is spectrally analyzed by a line-scanning spectrometer. To assign each pixel on the chip with the dimensions (x, λ) to a measurement point (channel) in the 3D cube with the dimensions (x, y, λ), the measured data need to be rearranged to the original image. Therefore, the correlation between the pixels of the detector and the channels of the image has to be determined (figure 3, step (e)–(f)). This was achieved by observing an unambiguous test pattern and identifying the position of each channel of the test pattern on the detector.
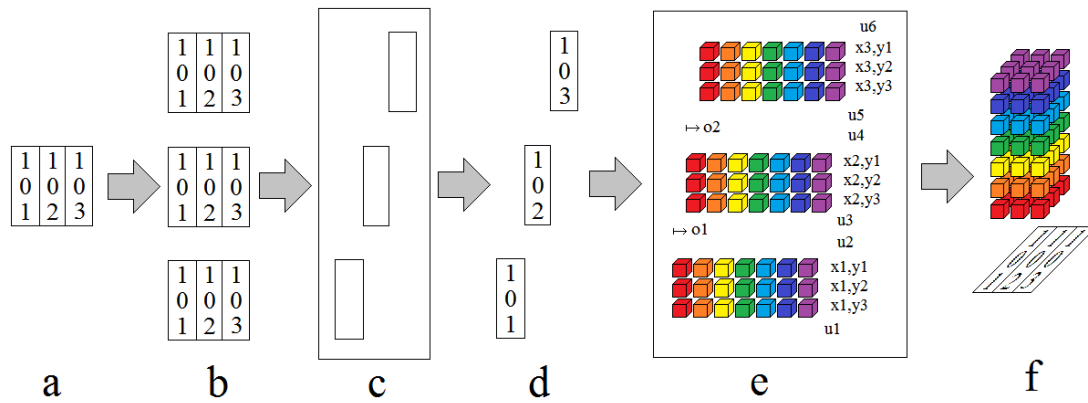
Figure 3. Schematic illustration of the imaging process of the 4D Imager where color indicates wavelength. The image (a) is multiple images with the help of the facet mirror (b). The different spatial information gets selected by a customized aperture (c). The selected data (d) are entering a line-scanning spectrometer where the single pixels are spectrally resolved (e). This data can be rearranged to get the spectral snapshot imaging voxels (f). Details of (e): between two sets of channels, such as (x_1, y_m) and (x_2, y_m), a few channels cannot be used (u_n). According to the saw tooth shape of the entrance slit (c), the wavelength range of each set is slightly shifted (o_n) to the next set. The measurement data can be remapped (f) into voxels (x, y, λ).
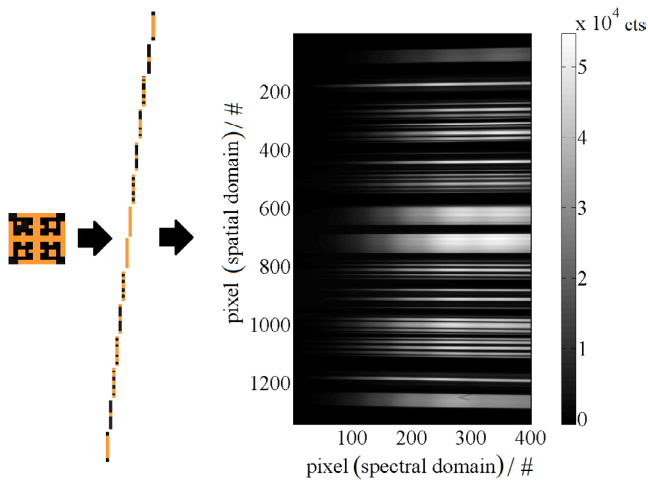

Figure 4. Measured raw data of the test pattern in counts (right side). For illustration purposes, the image and the selected parts after the aperture are shown on the left.

Due to image distortions within the spectrometer, the single channels are not imaged exactly along one pixel row in the spectral domain of the detector. An additional curve fitting individual for each channel on the detector along the signal in the spectral domain similar to Gao *et al* (2010) has been applied to correct these image distortions. In addition, the higher resolution data gained from the additional camera can be mapped to the spatial lower resolution spectral snapshot imaging measurement.

3.2. Wavelength calibration and optical bandwidth

The wavelength calibration of each channel has been achieved with the help of intrinsic lines of several pen ray lamps. The spectral range of a single channel enables a delta of 500 nm, e.g. 380 nm–880 nm in this configuration. However, as shown in figure 3(e), each set of channels is slightly shifted in the spectral domain. Thus, the common spectral range of all channels is 380 nm–800 nm with an optical bandwidth (FWHM) of 10 nm.
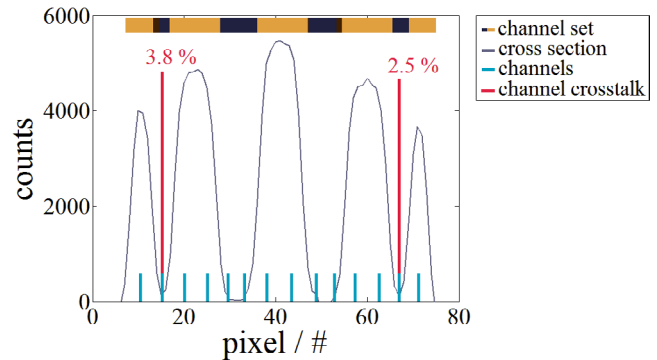

Figure 5. Shown is the measured cross-section of one set of channels in grey, the test pattern of this set of channels in yellow/ black and the used channels in blue. The maximum channel crosstalk is highlighted in red.

3.3. Radiometric calibration

The radiometric calibration of the 4D Imager has been performed by using a 210 mm integrating sphere based uniform light source traceable to the Physikalische Technische Bundesanstalt (PTB). The calibration uncertainty of this standard is 2% ($k = 2$) in the spectral range above 450 nm and is linearly increasing below 450 nm to 3.2% at 380 nm. The radiance distribution of the 65 mm exit port of the integrating sphere has to be very homogeneous within the FOV of the 4D Imager to ensure low calibration uncertainties. The inhomogeneity of the calibration source used is better than $\pm$ 0.20%. The 4D Imager has been calibrated at the measurement location so that no movement of the instrument between calibration and measurement is needed.

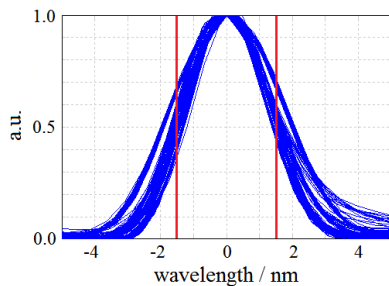### 3.4. Measurement results

A proof of concept measurement has been performed to analyze the spatial performance (channel separation) of the 4D Imager. As a measurement object, a 10 mm × 10 mm laser cut test pattern with 14 × 14 pixels has been backside illuminated with a tungsten lamp. To clarify the channel separation, the raw signal on the detector chip is presented in figure 4. The raw signal
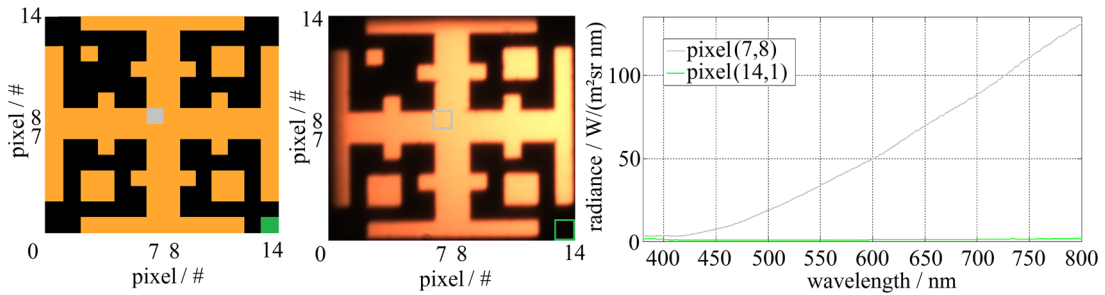
Figure 6. Results of the 14 × 14 pixel test pattern measurement. Left: Resolution of the spectral snapshot image. Center: Higher resolution image captured by the additional RGB camera. Right: Two representative measurement channels are illustrated in spectral radiance.

Figure 7. Left: Prototype of the 4D Imager equipped with an entrance optic for sky zenith measurements with a FOV of 0.5°. Right: Entrance optic for a wide angle FOV of 16.8°–73.5°. This optic can be mounted on the entrance optic for sky zenith measurements.

Figure 9. Radiance measurement of a uniform spectral radiance calibration standard. The data shows good agreement in the spectral range 370 nm–470 nm. Below 370 nm the residual deviation is rising mainly due to insufficient signal to noise ratio.
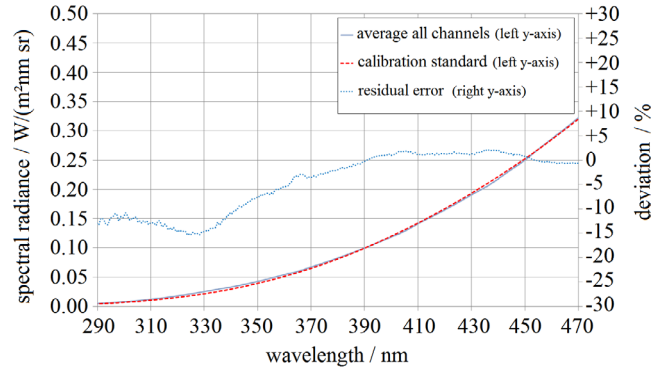

Figure 8. Optical bandpass of all 196 channels with the UV setup. A mean optical bandwidth (FWHM) of 3 nm has been achieved.
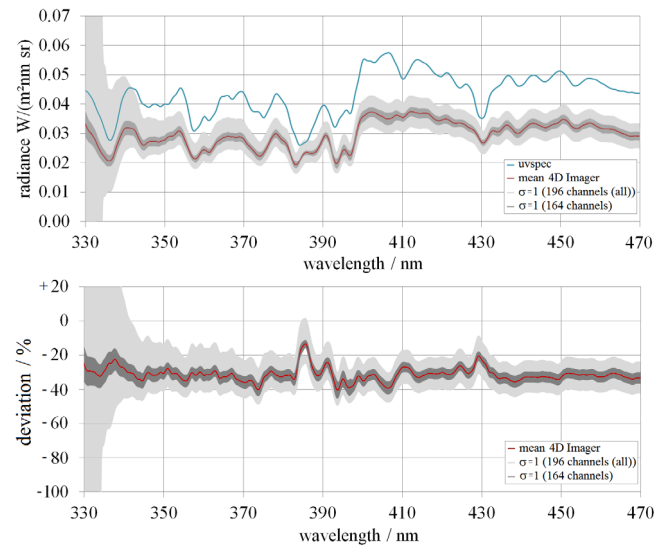
shows 14 imaged channel sets from which 14 channels can be used each. In principle, more detector pixels than could be used in each channel set. However, only 14 are clearly separated by a channel crosstalk of less than 4% (see figure 5). This investigation of the crosstalk is based on a perfectly aligned test pattern to the FOV of the 4D Imager. A slight offset, which might be present, leads to signals that appear like channel crosstalk.

The described calibration process has been applied to this raw data. Furthermore, the measured spectral snapshot imaging data have been mapped by the measurement software to the higher resolution image (0.58 megapixels) taken with the additional camera. In addition, the spectral data of two channels are illustrated in figure 6.

The measurement has been performed for all 196 channels simultaneously with an integration time of 3 s. No averaging or smoothing has been applied.

Figure 10. Solar zenith sky radiance measurements in the UV region from 330 nm–470 nm with 3 nm optical bandwidth (FWHM) of a clear sky (2017-02-15 14:15 UTC + 1 48°06′03.6″N 11°04′46.3″E) and ratio to UVSPEC generated data (convolved to 3 nm FWHM) are illustrated. In addition, the standard deviation of 196 channels (all) and 164 channels is shown. Some channels exhibit significant stray light, which can be recognized by the increase of the standard deviation, especially below 340 nm.

This measurement indicates a successful separation of the channels on the detector chip. However, to show the spectral radiometric capabilities of the new instrument, measurements
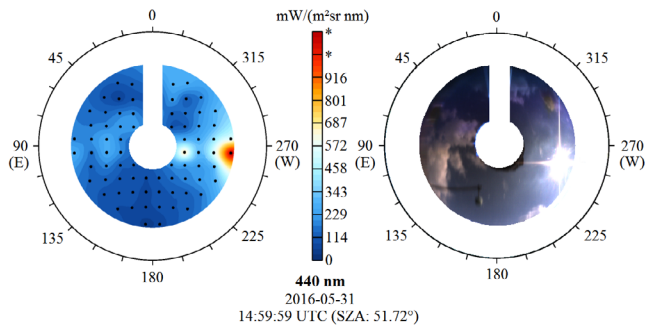
Figure 11. Left: Illustrated is a spectral sky radiance distribution at 400 nm (integration time of 1 s) in a color scale gradient representation. The black dots represent the central points of the single measurement channels. Right: Higher resolution RGB image captured by the additional camera.

of an object with a different spectral distribution compared to the calibration lamp have to be performed.

4. Application of the 4D Imager for spectral sky radiance measurements

For the analysis of the spectral radiometric performance of the 4D Imager and its capability in the UV, snapshot radiance measurements of the sky zenith were performed. Due to a large dynamic and high spectral stray light, solar radiation is difficult to measure, especially in the UV (Seckmeyer *et al* 2001). Hence, the optical design of the 4D Imager has been modified to access the UV spectral range and to achieve a smaller optical bandwidth (FWHM). Furthermore, the device has been equipped with an entrance optic to achieve a 0.5° FOV of zenith sky radiance, see figure 7, left.

4.1. Calibration

The calibration process was performed in the same manner as the VIS setup as described before. The calibration uncertainty of the standard increases linearly in the UV from 2% ($k = 2$) at 450 nm to 5% ($k = 2$) at 280 nm. A spectral range of 280 nm to 470 nm with a mean optical bandwidth of 3 nm (FWHM) was achieved (see figure 8). The measurements are corrected for stray light using a simple method similar to Riechelmann *et al* (2013), which is based on subtracting stray light signals from the measurement channel signals using detector channels that are not illuminated by the light source (see figure 3(e), channels *u*).

4.2. Measurement results

In figure 9 a measurement of a uniform spectral radiance calibration standard, which is as well traceable to PTB, has been performed to check the absolute radiometric capability of the measurement system. This standard is different to the used standard during calibration. The calibration uncertainty of this

standard is 3.5% ($k = 2$) in the spectral range above 350 nm and is linearly increasing with decreasing wavelength below 350 nm to 6.5% at 280 nm. The measurement results show an agreement with a deviation of less than ±3% in the spectral range 370 nm–470 nm. Below 370 nm the residual deviation is rising to about −15% in maximum mainly due to an insufficient signal to noise ratio.

In figure 10, the results of a clear blue sky zenith radiance measurement (2017-02-15 14:15 UTC + 1 48°06′03.6″N 11°04′46.3″E) are compared in the spectral range of 330 nm–470 nm to data processed with UVSPEC (Emde *et al* 2016). For this measurement scenario with a FOV of 0.5°, a constant spectral radiance distribution within the FOV is assumed. The UVSPEC data shown (input parameters UVSPEC: SZA 65.03°, SAA 28.47°, ozone 300 DU, albedo 0.02, altitude 599 m) are convolved to a comparable optical bandwidth of 3 nm (FWHM).

The measurement results show that all channels of the 4D Imager possess an offset of about −30% compared to the UVSPEC simulation results within the wavelength range 330 nm–470 nm. In addition, this offset shows a spectral variation due to not perfectly matched optical bandwidths for all channels at the Fraunhofer lines since every channel has a different FWHM (see figure 8). Furthermore, the standard deviation for the mean of 164 channels compared the standard deviation of 196 channels (all) shows that 32 channels exhibit significant stray light, especially below 340 nm.

In figure 11, a first measurement of a spectral sky radiance distribution using a wide angle entrance optic (FOV: 16.8° to 73.5°) is shown. This entrance optic (see figure 6, right) is mirror based and its design is according to Chahl and Srinivasan (1997). The measurement was captured within an integration time of 1 s.

5. Discussion and conclusions

Spectral snapshot imaging measurements have been performed with the 4D Imager, which is a new type of IFS technology. This technology is based on only a few optical parts which key component is a facet mirror that duplicates the object image. For the spectral analysis, a line-scanning spectrometer can be used. Hence, the spectral range and resolution of this technology is defined by the design of the spectrometer (l/mm of the grating, etc) whereby applications in the UV are also possible. These are the key advantages compared to other IFS approaches. The achievable spatial resolution can be as well designed with freedom since it depends on the number of facets, the detector resolution and the quality of the image selection process (customized aperture) connected with the imaging quality of the line-scanning spectrometer. The challenge of this technology is to image the duplicated images precisely on the entrance slit of the line-scanning spectrometer to support the selection process. An overview of the 4D Imager compared to different IFS technologies is presented in table 1.

Table 1. Overview of some IFS technologies with respect to its advantages and disadvantages.

	IFS-M	IFS-F	4D Imager
Advantage	- Since it is mirror based the spectral range is not limited	- Freedom in the FOV design since every fiber can be separately aligned - Freedom in the spectral design since standard line-scanning spectrometer can be used. In principle multiple line spectrometers can be combined	- Only a few optical parts are needed - Freedom in the spectral design since standard line-scanning spectrometer can be used - Since it is mirror based the spectral range is not limited
Disadvantage	- Many optical parts are needed since every sliced image needs a small mirror to be imaged at the pupil	- FOV is wavelength dependent due to wavelength dependent numerical aperture of the optical fibers	- Since the accessible wavelength range is shifted, for each set of channels which correspond to one facet, the useable common wavelength range is reduced compared to other techniques. It is reduced by the detector pixels which correspond to the width of a single entrance slit multiplied by the amount of facets
	- Hard to align since every mirror has to be aligned individually	- Movement of the measurement system can change the responsivity of the single measurement channels (fiber movement) - Different fibers are needed for the full spectral range from UV to IR - Amount of channels is limited mechanical by the number of fibers which means increase in measurement channels will be linear in increase of effort	- Due to the image multiplication and selection process only a part of the incoming available signal can be used (fraction is given by the number of facets)
Challenge	- Alignment of the system is non-trivial - Amount of measurement channels is difficult to increase since due to the many optical parts an optical imaging with many channels and acceptable image distortions is difficult to achieve	- Manufacturability of the fibers - Light coupling into the fiber	- A precise and unique entrance slit for the line spectrometer is needed
Resolution channel- crosstalk	$100 \times 100 \times 25$ (x, y, λ) Unknown (Gao *et al* 2009)	113×875 (x, λ) Unknown (Riechelmann *et al* 2013)	$14 \times 14 \times 400$ (x, y, λ) <4%

In this paper, proof of concept radiance measurements of a $10\,\text{mm} \times 10\,\text{mm}$ test pattern with a distance of 1 m and a spatial resolution of 14×14 channels (196) are shown. A channel crosstalk of less than 4% was attained. The channel crosstalk could be even smaller since the investigated signal is a mixture of the real channel crosstalk (optical imaging performance) and the alignment of the test pattern to the FOV of the 4D Imager. The device has been radiometrically calibrated, traceable to PTB, in the spectral range of $380\,\text{nm}$–$800\,\text{nm}$ with an optical bandwidth of $10\,\text{nm}$ (FWHM). Furthermore, the spectral snapshot imaging data (196 channels) have been mapped with a higher resolution RGB image that was captured by an additional facet and camera.

To demonstrate the spectral capabilities of this technology, spectral zenith sky radiance measurements in the UV region have been performed. Therefore, the prototype was adapted for a spectral range of $280\,\text{nm}$–$470\,\text{nm}$ with a mean optical bandwidth of $3\,\text{nm}$ (FWHM), a FOV of $0.5°$ and 196 channels. To check the radiometric capabilities of the measurement system a radiance measurement of a calibration standard was carried out. The results show a good agreement with a residual deviation of less then $\pm 3\%$ in the spectral range $370\,\text{nm}$–$470\,\text{nm}$ where sufficient signal to noise ratio is given by the used calibration standard. After this validation a spectral zenith sky radiance measurement was realized. The comparison of this measurement with UVSPEC generated data showed an

average offset of −30% in the range of 330 nm–470 nm. The reason for this deviation could not been determined exactly.

The uncertainty of any radiation measuring instrument is given by the combined calibration and measurement uncertainty. When comparing with modeled values, the uncertainty of the model and its input parameters must be considered as well. The UVSPEC model uncertainty is mainly dominated by the input parameters, e.g. aerosol characteristics of the atmosphere. This uncertainty has been investigated by Cordero *et al* (2013) for spectral UV irradiance. He found uncertainties for the UV–A range of about 3% for unpolluted atmospheres and about 5% for polluted atmospheres if realistic input uncertainties are assumed. The publication from van Weele *et al* (2000) showed that a difference of up to 20% at 305 nm between different UV models exists. Mayer *et al* (1997) found systematic differences between irradiance measurements and the UVSPEC model in the range between −11% to +2% for wavelengths between 295 nm and 400 nm and solar zenith sky angles up to 80°. The uncertainty of spectral UV irradiance measurements have been systematically assessed by Bernhard and Seckmeyer (1999) and found to be about 13% at 300 nm under ideal circumstances. Such uncertainties were later confirmed with a Monte-Carlo-approach by Cordero *et al* (2013). Pissulla *et al* (2009) showed that five independent calibrated systems exhibit a spectral radiance difference to UVSPEC between 3% and about 35%.

This suggests that an offset of −30% for spectral radiance is not very good, but still in the range of an acceptable agreement between the UVSPEC model and the 4D Imager. Furthermore, this comparison between UVSPEC and the 4D Imager measurement is based on the assumption of a clear sky, which might be not the case during the measurement (2017-02-15 14:15 UTC + 1 48°06′03.6″N 11°04′46.3″E).

It should be noted that the measurement showed that 36 channels exhibit significant stray light, especially below 340 nm. This is mainly caused by the prototype using an optical table setup at which the spectrometer housing was not yet completely light tight.

In this publication we do not want to show the possible endpoint of longer development, but just want to describe a proof of a new concept. The measurement results show the potential of the 4D Imager technology to measure spectral radiance using snapshot imaging. However, for high accuracy measurements, especially in the UV, a fixed setup with optimized light traps and a machine processed spectrometer housing would be needed. The optical table-based prototype used for these measurements clearly showed its limits when using it outdoors.

Acknowledgments

ORCID iDs

Ralf Zuber https://orcid.org/0000-0001-7794-9730

References

Bernhard G and Seckmeyer G 1999 Uncertainty of measurements of spectral solar UV irradiance *J. Geophys. Res.* **104** 14321–45

Bianco P, Pisani M and Zucco M 2010 High throughput, compact imaging spectrometer *Int. Conf. on Space Optics ICSO 2010*

Brown A J 2006 Spectral curve fitting for automatic hyperspectral data analysis *IEEE Trans. Geosci. Remote Sens.* **44** 1601–8

Brown A J, Hook S J, Baldridge A M, Crowley J K, Bridges N T, Thomson B J, Marion G M, de Souza Filho C R and Bishop J L 2010 Hydrothermal formation of clay-carbonate alteration assemblages in the Nili Fossae region of Mars *Earth Planet. Sci. Lett.* **297** 174–82

Brown A J, Sutter B and Dunagan S 2008 The MARTE VNIR imaging spectrometer experiment: design and analysis *Astrobiology* **8** 1001–11

Chahl J S and Srinivasan M V 1997 Reflective surfaces for panoramic imaging *Appl. Opt.* **36** 8275–85

Content R 1997 New design for integral field spectroscopy with 8-m telescopes *Proc. SPIE* **2871** 1295–305

Cordero R R, Seckmeyer G, Alessandro D, Fernando L and David L 2013 Monte Carlo-based uncertainties of surface UV estimates from models and from spectroradiometers *Metrologia* **50** L1

Davis C O *et al* 2002 Ocean PHILLS hyperspectral imager: design, characterization, and calibration *Opt. Express* **10** 210–21

Emde C *et al* 2016 The libRadtran software package for radiative transfer calculations (version 2.0.1) *Geosci. Model Dev.* **9** 1647–72

Gao L, Kester R T, Hagen N and Tkaczyk T S 2010 Snapshot image mapping spectrometer (IMS) with high sampling density for hyperspectral microscopy *Opt. Express* **18** 14330–44

Gao L, Kester R T and Tkaczyk T S 2009 Compact image slicing spectrometer (ISS) for hyperspectral fluorescence microscopy *Opt. Express* **17** 12293–308

Gehm M E, John R, Brady D J, Willett R M and Schulz T J 2007 Single-shot compressive spectral imaging with a dual-disperser architecture *Opt. Express* **15** 14013–27

Gupta N and Voloshinov V 2004 Hyperspectral imager, from ultraviolet to visible, with a KDP acousto-optic tunable filter *Appl. Opt.* **43** 2752–9

Hagen N and Kudenov M W 2013 Review of snapshot spectral imaging technologies *Opt. Eng.* **52** 090901

Hardeberg J Y, Schmitt F and Brettel H 2002 Multispectral color image capture using a liquid crystal tunable filter *Opt. Eng.* **41** 2532–48

Henault F, Bacon R, Content R, Lantz B, Laurent F, Lemonnier J-P and Morris S L 2004 Slicing the universe at affordable cost: the quest for the MUSE image slicer *Proc. SPIE* **5249** 134–45

Hu P, Lu Q, Shu R and Wang J 2005 An airborne pushbroom hyperspectral imager with wide field of view *Chin. Opt. Lett.* **3** 689–91

Laurent F, Henault F, Renault E, Bacon R and Dubois J P 2006 Design of an integral field unit for MUSE, and results from prototyping *Publ. Astron. Soc. Pacific* **118** 1564–73

Mathews S A 2008 Design and fabrication of a low-cost, multispectral imaging system *Appl. Opt.* **47** F71–6

Matsuoka H, Kosai Y, Saito M, Takeyama N and Suto H 2002 Single-cell viability assessment with a novel spectro-imaging system *J. Biotechnol.* **94** 299–308

Mayer B, Seckmeyer G and Kylling A 1997 Systematic long-term comparison of spectral UV measurements and UVSPEC modeling results *J. Geophys. Res.* **102** 8755–67

Pissulla D *et al* 2009 Comparison of atmospheric spectral radiance measurements from five independently calibrated systems *Photochem. Photobiol. Sci.* **8** 516–27

Riechelmann S, Schrempf M and Seckmeyer G 2013 Simultaneous measurement of spectral sky radiance by a non-scanning multidirectional spectroradiometer (MUDIS) *Meas. Sci. Technol.* **24** 125501

Seckmeyer G, Bais A, Bernhard G, Blumthaler M, Booth C, Disterhoft P, Eriksen P, McKenzie R, Miyauchi M and Roy C 2001 Instruments to measure solar ultraviolet irradiance. Part 1: spectral instruments *Global Atmosphere Watch Report* No. 125 World Meteorological Organization (WMO)

Sigernes F *et al* 2012 Hyperspectral all-sky imaging of auroras *Opt. Express* **20** 27650–60

van Weele M *et al* 2000 From model intercomparison toward benchmark UV spectra for six real atmospheric cases *J. Geophys. Res.* **105** 4915–25

Wagadarikar A, John R, Willett R and Brady D 2008 Single disperser design for coded aperture snapshot spectral imaging *Appl. Opt.* **47** B44–51

Zuber R 2015 Spetroskopiesystem *Ger Patent* 102013112376